Science of the Total Environment 550 (2016) 1141–1151

Contents lists available at ScienceDirect

Science of the Total Environment

journal homepage: www.elsevier.com/locate/scitotenv

Mineralogical control on arsenic release during sediment–water interaction in abandoned mine wastes from the Argentina Puna

N.E. Nieva [a], L. Borgnino [a,b], F. Locati [a], M.G. García [a,b,*]

[a] Centro de Investigaciones en Ciencias de la Tierra (CICTERRA), CONICET - UNC
[b] FCEFyN Universidad Nacional de Córdoba, Córdoba, Argentina

HIGHLIGHTS

- Sulfide mine wastes are accumulated in La Concordia mine, Argentina Puna.
- The wastes are a source of arsenic, metals and acidity to the nearby ecosystems.
- As minerals are Fe sulfides, jarosite, (hydrous)sulfates and scarce arsenates.
- Intense evaporation leads to precipitation of readily soluble efflorescences.
- A high proportion of As remains adsorbed onto Fe (hydr)oxides

GRAPHICAL ABSTRACT

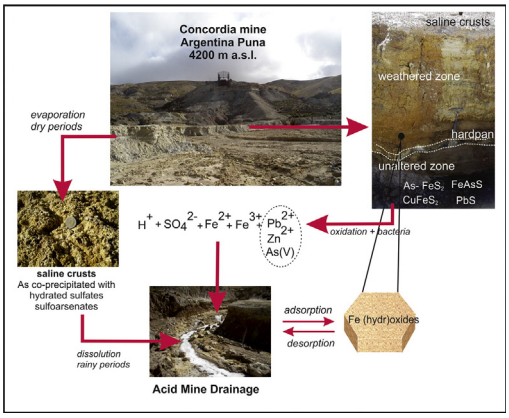

ARTICLE INFO

Article history:
Received 16 October 2015
Received in revised form 19 December 2015
Accepted 22 January 2016
Available online xxxx

Editor: F.M. Tack

Keywords:
Concordia mine
Central Andes
As jarosite
Sulfate efflorescences
Sulfide oxidation

ABSTRACT

The sulfide-rich residues of La Concordia mine, Argentina Puna, are accumulated in tailing dams that remained exposed to the weathering agents for almost 30 years. In such period of time, a complex sequence of redox and dissolution/precipitation reactions occurred, leading to the gradual oxidation of the wastes and the formation of weathering profiles. The sources of arsenic in the wastes were analyzed by XRD and SEM/EDS analysis while a standardized sequential extraction procedure was followed to define solid As associations. In addition, the release of As during sediment–water interaction was analyzed in a period of 10 months. The results indicate that primary As-bearing minerals are arsenian pyrite and polymetallic sulfides. As-jarosite and scarce arsenates are the only secondary As-bearing minerals identified by XRD and SEM/EDS. However, the rapid release (i.e., <1 h) of arsenic from suspensions of the studied sediments in water, seems to be associated to the dissolution of highly soluble (hydrous)sulfates, as it was determined in samples of the efflorescences that cover the entire site. Contributions from the more abundant As-jarosite are also expected in longer periods of sediment–water interaction, due to its low rate of dissolution in acid and oxic conditions. Finally, near 30% of As remains

* Corresponding author at: Av. Velez Sarfield 1611, Ciudad Universitaria - Córdoba (X5016GCA), Argentina.
E-mail address: gabriela.garcia@unc.edu.ar (M.G. García).

http://dx.doi.org/10.1016/j.scitotenv.2016.01.147
0048-9697/

adsorbed onto Fe (hydr)oxides thus representing a hazardous reservoir with the potential of mobilizing As into porewaters and streamwaters if the acidic and oxidizing conditions that predominate in the region are altered.

1. Introduction

The western border of South America is one of the most active volcanic areas in the world. During the Middle Miocene, an important back-arc volcanism affected the Puna plateau of NW Argentina, south-central Andes (Coira et al., 1993; Coira and Viramonte, 1999; Matteini et al., 2002) that produced significant volcanic complexes and calderas associated with polymetallic mineralization (i.e., Petrinovic et al., 1999; Riller et al., 2001). A number of small mining districts spread in the Puna region, discontinuously exploited these hydrothermal ores since the Spanish colonization until the middle 1990's, when they were all definitively closed without executing appropriate practices of site remediation.

When sulfidic mine wastes are exposed to the weathering agents and to the action of microorganisms, a highly acidic drainage, rich in dissolved metal(oid)s and sulfate is generated (i.e., Jamieson, 2011; Lottermoser, 2010; Nordstrom and Alpers, 1999). The main process involves the oxidation of the parent sulfide and the subsequent precipitation of secondary minerals such as sulfates, hydroxysulfates, oxides and arsenates. During such process, elevated concentrations of potentially toxic elements are released to the water and then incorporated into a cycle that includes the precipitation/dissolution of efflorescent and more stable salts as well as adsorption/desorption from Fe or Al (hydr)oxide sites (Lottermoser, 2010).

Arsenic is one of the most hazardous contaminants associated to acid mine drainage (AMD) because it is highly mobile over a wide range of pH. Therefore, As can be transported for long distances in solution, in the form of the As(V) and As(III) species $H_2AsO_4^-$, $HAsO_4^{2-}$ and $H_3AsO_3^0$ depending on the water redox conditions. Arsenate compounds are generally less mobile and less toxic than arsenite (Smedley and Kinniburgh, 2002).

In arid regions impacted by acid drainage, arsenic may co-precipitate as an impurity along with a wide variety of secondary minerals, such as schwertmannite and jarosite (e.g., Nordstrom and Alpers, 1999; Bigham and Nordstrom, 2000) as well as metal arsenates and sulfoarsenates (Drahota and Filippi, 2009). Co-precipitation refers to the formation of a mineral phase in which As precipitate as a stoichiometric compound such as scorodite ($FeAsO_4 \cdot 2H_2O$), as a poorly ordered phase of variable composition such as pitticite (FeIII–SO_4–As_2O_5–H_2O), or as a solid-solution impurity in some other mineral species (Carlson et al., 2002). Thus, the release of As from these phases strongly depends on the compound solubility. In the highly acidic conditions predominating in these systems, desorption from Fe (hydr)oxides is almost negligible. Secondary minerals that are more susceptible to dissolution are simple hydrous metal sulfates, while Fe or Al hydroxysulfates are relatively insoluble (Lottermoser, 2010). Fe arsenates in turn, are more insoluble than Fe or Al hydroxysulfates in acid environments (Langmuir et al., 2006). Secondary phases may precipitate either as amorphous, poorly crystalline or well-crystallized products, cementing and encrusting tailings particles on a laterally extensive or discontinuous scale (Lottermoser and Ashley, 2006). These phases may act as sinks of contaminants as they retain them by adsorption or co-precipitation, processes that are particularly important in regions with elevated rates of evaporation. However, in arid regions, this function may be limited because some of these salts are highly soluble and thus, they rapidly dissolve during occasional rainfall events, releasing metals and metalloids that can be carried to streams as ionic species in solution. The environmental relevance of the flush-out effect in AMD systems is well documented (e.g. Nordstrom and Alpers, 1999). According to Frau (2000), the longer the dry period, the more intense the environmental impact during the subsequent wet period.

In this paper, we analyze the sources of As in the abandoned mine wastes accumulated in La Concordia mine, in the arid region of the Argentina Puna as well as its release during sediment–water interaction. Our goals were to analyze the distribution of arsenic concentrations along weathering profiles formed in the abandoned tailing dams, to identify the main As-bearing minerals and to assess the control of the mineralogy on the release of arsenic in the impacted site. The results obtained here may contribute to the understanding of arsenic bioavailability in high altitude and arid environments.

2. Study area

La Concordia mine is located in the Puna region of Salta province, NW Argentina (24°12′ S y 66°24′ W; 4200 m a.s.l.), 15 km NW the village of San Antonio de los Cobres (Fig. 1). Climatic conditions are extreme due to the altitude. Climate is semiarid; wide daily temperature variations and rainfall concentrated in one season are typical features. Annual average precipitation is 200 mm and occurs between November and February (late spring and summer of the southern hemisphere). The mean annual temperature in the area is 8.7 °C, but temperatures as high as 40 °C can be recorded during summer while in winter night temperatures of about −25 °C are frequent.

La Concordia was mined for Pb, Ag and Zn until 1986 when it was closed. Reserves were estimated in 40,000 t, with grades that averaged 5.6% Pb, 491 g/t Ag, 1.26% Zn, and 0.6% Cu (Argañaraz et al., 1982). The epithermal mineralization is genetically linked to a Miocene dacite dome. The country rock corresponds to clusters of Pirgua Subgroup, which is considered the most auspicious for finding veins associated with highly anomalous gold content. The hydrothermal alteration affecting the dacite is sericitic and argillic with patches of intense silicification. In areas affected by silicification, strong anomalies of Au, Ag and Sb were found. Paragenesis consists predominantly of argentiferous tetrahedrite $(Cu,Ag)_3SbS_3$, galene (PbS), sphalerite (ZnS), chalcopyrite ($CuFeS_2$), and auriferous pyrite (FeS_2), usually associated with quartz. Arsenopyrite (FeAsS), bournonite ($PbCuSbS_3$), marcasite (FeS_2), pirargirite (Ag_3SbS_3), zinckenite ($Pb_9Sb_{22}S_{42}$), semseyite ($Pb_9Sb_8S_{21}$) and jamesonite ($Pb_4FeSb_6S_{14}$) are also present as accessory minerals. Secondary minerals are gypsum ($CaSO_4 \cdot 2H_2O$), limonite ($FeO(OH) \cdot nH_2O$), kaolinite ($Al_2(Si_2O_5)(OH)_4$), melanterite ($FeSO_4 \cdot 7H_2O$), halotrichite ($FeAl_2(SO_4)_4 \cdot 22H_2O$), and anglesite ($PbSO_4$) (Zappettini, 1990).

During the mining activities, the tailings repository consisted of four tailings cells (TI, TII, TIII, and TIV) that covered an area of 8814 m^2, and that were constructed as a series of embankments along the narrow valley of the Concordia Creek. No basal liner was setup beneath the tailings and the cells were left uncovered after closure of the plant in 1986. The sediments accumulated in the tailings were affected by evaporation and weathering for at least 30 years, leading to the formation in depth of layers that can be differentiated according to texture and color criteria. In a previous work, Kirschbaum et al. (2012) described the stratigraphic characteristics of these profiles. According to these authors, they consist of an irregular succession of sandy and clay layers, where the uppermost layers show more evidences of oxidation while bottom sediments are generally unaltered and water saturated. Ochre deposits, including hardpan crusts (5–10 cm thick) are usually observed filling fissures in the wall rocks and on the tailings surface acting as a barrier that prevents from rapid oxidation.

Yellowish and white efflorescent salts cover almost the entire streambed and the surface of the tailings. Several Fe and Pb sulfates such as rozenite ($FeSO_4 \cdot 4H_2O$), jarosite ($KFe_3(SO_4)_2(OH)_6$), szomolnokite ($FeSO_4 \cdot H_2O$), anglesite ($PbSO_4$) and ferricopiapite

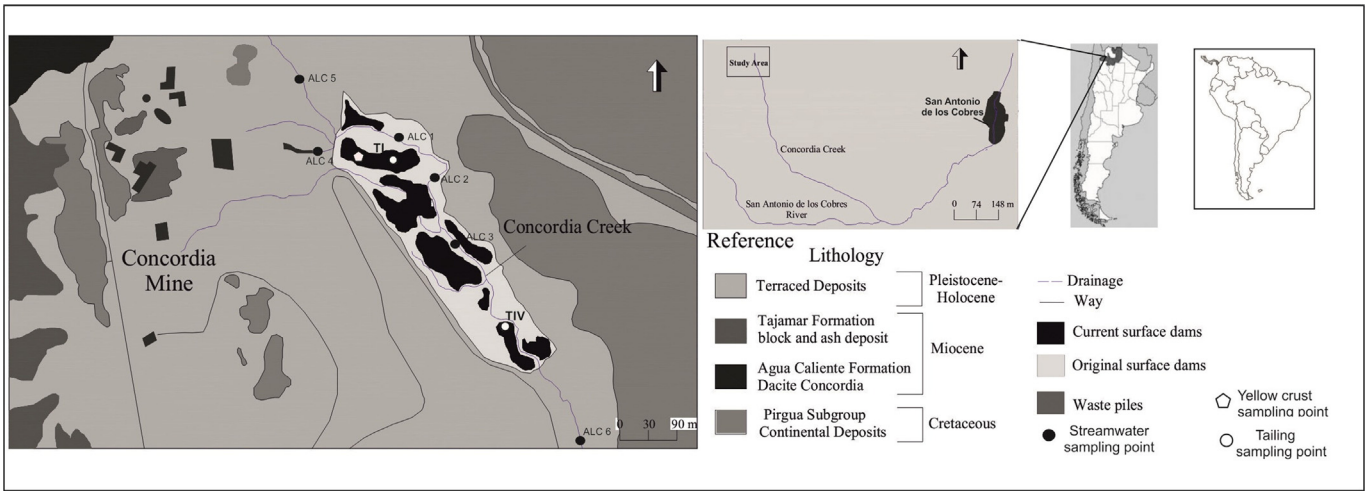

Fig. 1. Map of La Concordia mine site showing the location of water and sediment sampling points.

$(Fe_{2/3}Fe_4(SO_4)_6(OH)_2 \cdot 20(H_2O)$ were identified in these salts (Kirschbaum et al., 2012).

Signs of AMD are clearly observed in the Concordia creek (Fig. 1), a 14 km long stream whose headwaters are located in the mine adits. The stream discharges into the San Antonio River, the main water supply of the San Antonio de los Cobres village (~6100 inhabitants). During the dry season (i.e., the austral winter), the creek completely infiltrates about 5 km downstream the tailings, and outcrops about 3 km upstream its discharge into the San Antonio River. This place is known as Baños de Pompeya, and corresponds to a geothermal system as described by Pesce and Miranda (2003). A previous chemical characterization of the streamwater near the mine revealed the occurrence of highly acidic waters ($3 < pH < 4$) with elevated concentrations of As, B, Cd, Mn, Pb, and Zn (Kirschbaum et al., 2012).

3. Methodology

3.1. Profiles description and sampling

Sediment samples were collected from exposed depth profiles in tailings I and IV (Fig. 1). The gradual oxidation that affected the sediments accumulated into the tailing dams lead to the formation of several layers that were differentiated mainly through color, consistency and grain-size criteria.

Depth profile in tailing I (Fig. 2a) consists of a ~200 cm depth succession of silty and sandy layers, that have been divided into five layers, and sampled for chemical and mineralogical analysis. The uppermost 60 cm thick layer (TI-A) consists of yellowish sands and silts that overlay a 20 cm thick layer of brown yellowish silts (TI-B). A laterally discontinuous layer ($TI\text{-}B_2$) was also recognized at the base of layer TI-B and consists of a 10 cm thick layer of whitish fine silts. Below $TI\text{-}B_2$, the layer TI-C consists of laminated yellow greenish silts that were not saturated at the moment of sampling, but showed some hydromorphic characteristics that suggest periodic waterlogged conditions. The deepest layer TI-D consists of a massive dark gray sequence of fine silts that were completely saturated at the moment of sampling.

Depth profile in tailing IV (Fig. 2B) consists of a ~200 cm depth succession of coarse to fine sands, which were completely dry at the moment of sampling. Three layers were distinguished in this profile: the uppermost layer is 60 cm thick, and consists of white yellowish fine sands (TIV-A). From 60 to 105 cm depth, the intermediate layer TIV-B was identified. It is composed of coarse subangular clasts spread in a coarse yellow to brown sand matrix. From 105 cm up to the bottom of the profile, sediments correspond to red coarse gravels deposited by the creek before the building of the dams.

Samples of the saline crusts that cover the streambed as well as the surface and exposed walls of the tailings were also collected. Crusts were separated according their predominating color. Yellow crusts cover almost the entire site, mostly the streambed and surface of the tailings, while red crusts were collected from the exposed wall in tailing I. Some aggregates of blue salts disseminated in the layer TIV-B were also collected for chemical and mineralogical analysis (Fig. 2).

All samples were collected using a Teflon shovel in order to avoid metal contamination, double bagged in sealed low O_2 diffusion plastic bags and transported to the laboratory refrigerated at 4 °C. Before analysis, samples were air-dried and sieved through a 230 mesh; the fraction <63 μm was used for all determinations and experiments carried out in this work.

3.2. Water sampling and field determinations

Five streamwater samples were collected from the Concordia Creek, in the stretch affected by mine wastes, while one sample (ALC-5) was taken from a small tributary, a few meters upstream its confluence with La Concordia creek (Fig. 1). Sampling was carried out in June 2014, when baseflow conditions prevailed. The latter ensures a better identification of potential contributions from different water sources and minimizes the effect of dilution caused by rainfall.

Field determinations consisted of pH, electrical conductivity (EC), total dissolved solids (TDS), temperature, oxidation reduction potential (ORP), and alkalinity measurements. The pH was measured using a Metrohm 827 portable pH-meter with a combined electrode and integrated NTC temperature sensor for automatic temperature compensation. ORP was determined with a Combined Pt-ring electrode that contains a Ag/AgCl internal reference electrode. The ORP values were adjusted with respect to hydrogen electrode and expressed as Eh. Electrical conductivity (EC) was measured using a Hach portable conductivity meter, and alkalinity was determined in 100 ml samples by titration using 0.16 N H_2SO_4 and bromocresol green–methyl red as end point indicator (Hach Co).

Immediately after collection, samples were filtered in situ through 0.22 μm cellulose acetate membrane filters (Millipore Corp.) and divided into two aliquots. The filtration equipment was repeatedly rinsed with sample water prior to filtration. Aliquots used for major cations and trace elements determination (15 ml) were acidified to $pH < 2$ with ultrapure HNO_3 (>99.999%, redistilled) and stored in pre-cleaned polyethylene bottles. The remaining 20 ml aliquot was stored in polyethylene bottles, without acidifying, at 4 °C for the determination of major anions.

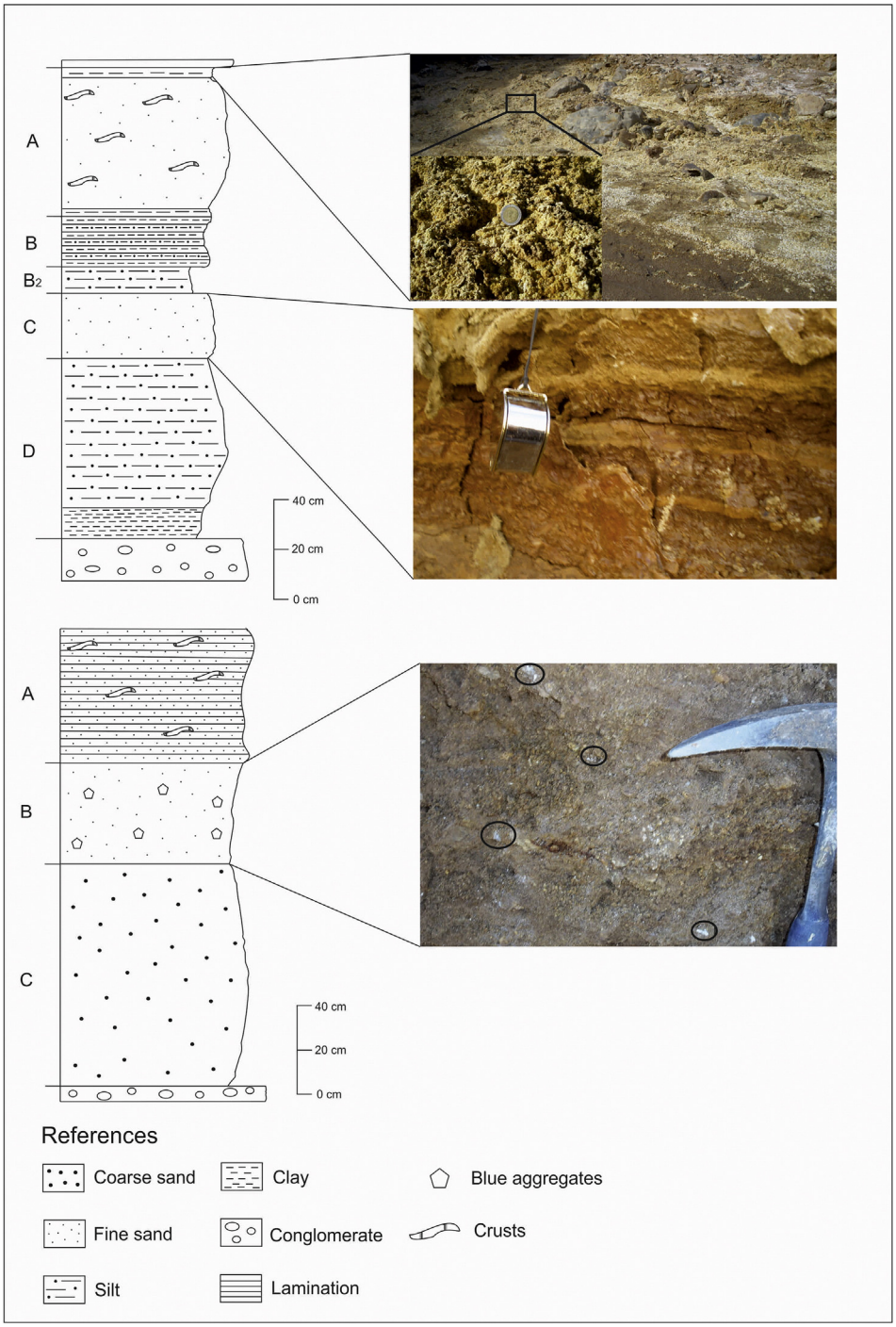

Fig. 2. Sedimentological characteristics of the weathering profiles formed in tailings I and IV. Pictures show the saline crusts and aggregates found in the tailings. The upper photograph shows the yellow efflorescences that cover the entire surface of tailings and the Concordia streambed. The intermediate photograph show the red crusts that cover the profile's walls, while the bottom image corresponds to aggregates of blue salts found in tailing IV. (For interpretation of the references to color in this figure legend, the reader is referred to the web version of this article.)

3.3. Chemical analysis

The near-total chemical composition of the tailing's layers was determined in sediment extracts obtained after acid digestion. Briefly, a 0.25 g split is heated in HNO_3–$HClO_4$–HF to fuming and taken to dryness. The residue is dissolved in HCl and solutions are analyzed by ICP-OES (Spectro — model Arcos). The validity of the results for major, minor, and trace elements was checked against measurement of OREAS25A-4A and OREAS45E standards, which were carried out along with sample analysis (Table 2).

The chemical composition of saline crusts and aggregates was determined in extracts obtained after dissolution in MilliQ water. About 1.00 g of sample was suspended in 50 ml of MilliQ water and stirred for 1 h. The obtained leachate was separated and analyzed by ICP-OES analysis (Spectro — model Arcos). The remaining residue was dried as weighted in order to calculate the mass of dissolved salts.

Anions (Cl^-, F^-, NO_3^-, and SO_4^{2-}) in streamwater samples were determined by chemically suppressed ion chromatography with conductivity detection (Thermo Scientific™ Constametric 3500), while cations and trace elements were measured by ICP-MS (Agilent

7500cx). Deionized water (18 MΩ cm^{-1} MilliQ, Millipore Corp.) was used for all solutions and dilutions. For all elemental determinations performed by ICP-MS, calibration curves were run before and after each sample series (8–10 samples including blanks and in-between calibration checks). The calibration solutions covered the range of concentration in the samples and were prepared in ultrapure 2% HNO_3 from certified stock solutions. Sample blanks were analyzed for correction of background effect on instrument response. Metal concentrations in unknown solutions were calculated with the ChemStation spectrometer software. Detection limits were calculated as three standard deviation of the instrument response from 10 replicates of blank solutions.

3.4. Mineralogical determinations

Minerals in the <63 μm size-fraction of the samples were identified by X-ray diffraction (XRD) and scanning electron microscopy/energy-dispersive X-ray spectroscopy (SEM/EDS) measures. XRD analysis was performed with a PANalytical X'Pert Pro diffractometer operating at 40 kV and 40 mA using Cu-Kα radiation. XRD data were obtained for random samples in the 2θ range from 5 to 70° (step size: 0.02; 3 s/step) with a detection limit of 1%. Phase identification and Rietveld quantitative phase analysis were carried out using the X'Pert High Score Plus v3.0e software package by PANalytical.

SEM/EDS analysis was performed with a Carl Zeiss Sigma FE-Scanning Electron Microscope. Samples (gently disaggregated with a pestle and mortar) were mixed with Epofix resin and hardener. The samples were left within a pressure vessel for approximately 12 h before being backfilled with araldite resin, and cured in a drying oven (50 °C, ≥4 h). Once set, the sample was polished and subsequently carbon coated before being measured. In addition, SEM was coupled with focused energy dispersive X-Ray analysis (EDS, AZTec, Oxford) in order to perform the elemental semi-quantification. The detection limit of EDS analysis was about 0.1% for arsenic; the spatial resolution was about 1 μm.

3.5. Batch leaching experiments

Batch experiments were performed in order to evaluate the release of As throughout time in MilliQ water. The experiments we carried out by suspending ~1.00 g of dry sample in 50 mL of MilliQ water (pH 6.5) and continuously shaking using a rotator shaker. The suspensions were completely withdrawn after 1, 2, 5, and 10 h and 1, 3, 8, 15, 30, 84, 125, 176, 216 and 306 days of the start of the experiments, centrifuged at 5000 rpm for 15 min and then filtered through a 0.22 μm cellulose membrane filter for chemical analysis. The pH of the suspensions at the end of each step was registered before separating the supernatant. In all cases, final pH dropped to <4.0. After each step of extraction, the residue was re-suspended in 50 mL of MilliQ water (pH 6.5) and the procedure was repeated until the end of the experiment. Arsenic and some other trace elements were analyzed in acidified dilutions (1% HNO_3) by ICP-MS. Detection limit was 0.22 μg l^{-1} for As.

3.6. Sequential extraction

The sequential extraction procedure proposed by Dold (2003) was adapted in this study in order to identify the following phases present in the tailing profiles: 1) water soluble; 2) weakly adsorbed As; 3) strongly adsorbed As; 4) Fe (III) oxy-hydroxides (i.e., ferrihydrite; schwertmannite, etc.); 5) Fe (III) oxides (goethite, hematite, jarosite, etc.); 6) primary sulfides. The As content that remained in the residual fraction was calculated as: $[As]_{near\text{-}total} - \sum [As]_{steps1-6}$. Extractions 2 and 3 were proposed by Keon et al. (2001) to better identify the fractions of weakly and strongly adsorbed As respectively. The details of the procedure are indicated in Table 1. After each extraction, samples were centrifuged at 4000 rpm for 15 min. The obtained supernatants were filtered using 0.22 μm cellulose membranes and the chemical composition was determined by ICP-OES. Detection limit was 30 μg l^{-1} for As.

Table 1
Sequential extraction procedure used for this study. The sequence proposed by [1]Dold (2003) was adapted in order to include the steps corresponding to weakly and strongly adsorbed fractions proposed by [2]Keon et al. (2001).

Step	Extracted fraction	Reagents used
1	Water soluble: e.g., rozenite, pickeringite, gypsum	MilliQ water, shake for 1 h at room temperature[1]
2	Weakly adsorbed As	1 M $MgCl_2$; pH 8.0; 2 h; 25 °C[2]
3	Strongly adsorbed As	1 M NaH_2PO_4; pH 5.0; 16 and 24 h; 25 °C[2]
4	Fe(III) oxy-hydroxides (i.e., schwertmannite, ferrihydrite, etc.)	0.2 M NH_4-oxalate pH 3.0 shake for 1 h in darkness[1]
5	Fe (III) oxides (i.e., goethite, hematite, jarosite, etc.)	0.2 M NH_4-oxalate; pH 3.0; heat in water bath 80 °C for 2 h[1]
6	Primary sulfides	Combination of $KClO_3$ and HCl, followed by 4 M HNO_3 boiling[1]

4. Results

4.1. Chemical characterization of streamwaters

The physico-chemical parameters and the concentration of major ions and selected trace elements measured in the streamwater samples are shown in Supplementary Table 1.

Highly acidic pH values prevail in the analyzed stretch, where pH varies between 3.18 and 3.66. Electrical conductivity (EC) is elevated and remains almost constant in the flow direction, with an average value of 2.3 mS cm^{-1}. Oxidized conditions were determined along this stretch with Eh values that ranged between 311 and 410 mV.

The major chemical composition of the streamwater is dominated by the occurrence of elevated concentrations of SO_4^{2-} and null HCO_3^-. The concentrations of mayor ions remain nearly constant in the analyzed stretch, while trace elements such as As, Fe and Pb show a trend of decreasing concentrations in the flow direction. Interestingly, the sample collected in the creek tributary (ALC 5), show markedly lower element concentrations, probably because it is not in contact with the mine tailings.

The concentrations of arsenic exceed in several orders of magnitude the recommended guideline value for drinking waters set by the Argentinean and international regulations (10 μg l^{-1}; CAA, 2007; WHO, 2004). In the stretch dominated by AMD, concentrations vary from 5087 μg l^{-1} at the output of the mine adits to ~76 μg l^{-1} before the complete infiltration of the stream, a few meters downflow the tailing IV.

4.2. Chemical composition of tailings

The chemical composition of the layers described in the profiles of tailings I and IV and saline crusts is reported in Table 2. Most elements are more concentrated in the tailing I, where a bottom unaltered level is still present.

Most abundant trace elements throughout profile I are Zn, Cu, Pb, and As in order of decreasing abundance. In depth, it is observed a depletion of most elements in the bottom zone (layers TI-C and TI-D) whereas most elements are highly enriched in the thin layer TI-B_2. Processes such as co-precipitation and adsorption likely occur here because this layer seems to accumulate the elements leached from the overlying level. Due to its physical and chemical characteristics this layer can be clearly defined as a hardpan barrier. Lottermoser (2010) indicated that the effect of hardpan in tailings dams is to protect the underlying materials from further oxidation and to limit the generation of AMD and metal release by reducing the sediment's porosity and enhancing the accumulation of metals through adsorption and further co-

Table 2
Near-total composition (aqua regia extractable) of layers described in tailings I and IV and saline crusts. nd: not determined; bdl: below detection limit.

Sample	Na	K	Ca	Mg	Al	Fe	Ti	P	S	Cu	Pb	Zn	As
	%									mg kg^{-1}			
T-I													
TI-A	0.059	2.61	0.80	0.38	5.16	2.68	0.212	0.049	2.70	3405	5324	2826	1657
TI-B	0.060	3.46	0.94	0.46	6.92	3.85	0.230	0.048	5.10	3073	>10,000	3774	2119
TI-B2	0.063	2.74	1.04	0.42	5.98	4.90	0.178	0.076	5.80	4004	9619	4859	3101
TI-C	0.060	3.46	0.45	0.32	4.62	2.02	0.227	0.030	1.60	758	6032	1522	898
TI-D	0.053	3.50	0.22	0.41	5.57	3.15	0.245	0.043	3.10	1599	9980	3134	1752
T-IV													
TIV-A	0.053	2.32	0.51	0.30	4.29	0.89	0.222	0.007	0.80	86	1338	527	371
TIV-B	0.629	3.32	0.17	0.31	5.58	6.31	0.207	0.058	1.60	161	2602	258	1086
TIV-C	1.059	2.54	0.58	0.50	6.53	5.08	0.286	0.066	0.70	158	249	416	1043
Saline crusts													
Yellow crust	0.57	bdl	0.08	0.86	1.46	0.45	nd	nd	nd	1626	2468	5873	18
Red crust	1.19	0.28	0.06	1.87	0.05	20.69	nd	nd	nd	14,114	495	51,564	2339
Blue aggregates	5.85	0.39	0.10	11.92	12.73	1.23	nd	nd	nd	19,824	904	89,574	88
Reference materials													
Meas OREAS25A-4A	0.13	0.52	0.29	0.34	8.72	6.68	0.959	0.050	bdl	37.6	27.3	43.0	10.0
Meas OREAS45E	0.05	0.35	0.06	0.15	6.98	25.63	0.538	0.033	bdl	789.7	18.9	45.0	15.0
STD OREAS25A-4A (certified value)	0.13	0.48	0.31	0.33	8.87	6.60	0.977	0.048	0.051	33.9	25.2	44.4	nd
STD OREAS45E (certified value)	0.06	0.32	0.06	0.15	6.78	24.12	0.559	0.034	0.046	780.0	18.2	46.7	16.3

precipitation of secondary minerals. In addition, hardpan also serves as a barrier that limits metal-bearing particle migration.

In the profile of tailing IV, the more abundant elements are also Zn, Cu, Pb, and As, but their order of abundance differ in depth. Indeed, in the uppermost layer (TIV-A), Zn, Pb and As are fairly more abundant than Cu; in the intermediate layer TIV-B, As and Pb are the most abundant trace elements, followed by Zn and Cu. In the bottom layer (TIV-C), As remains the most abundant trace element followed in order of decreasing abundance by Zn, Cu and Pb. No hardpan layer was recognized in this profile.

The in-depth distribution of As in the profile of tailing I reveals that the higher As concentrations are found in the hardpan level (TI-B_2) and in the layer located immediately above (TI-B). Intermediate concentrations were measured in both, the uppermost and bottom layers. In tailing IV As concentrations are markedly lower compared with those determined in tailing I, with the highest concentration found in the bottom layer.

4.3. Mineralogical composition of tailings and efflorescences

The mineralogy of the tailing sediments and efflorescences reported in Table 4 corresponds to the crystalline phases identified by XRD. Silicates such as quartz, plagioclases, and illite, as well as pyrite are the main primary minerals determined along the depth profile in tailing I. In addition, grains of polymetallic sulfides and specially of As-bearing Fe and Pb sulfides were frequently observed by SEM/EDS analysis (see Supplementary Figs. 1 and 2 for X-ray diffractograms, SEM images and EDS spectra). Quartz is the most abundant mineral in the profile of tailing I (>47% of the total mineral content), followed by Illite (25.1–36.6%). Plagioclase is scarce and it was only quantified in layers TI-B_2 and TI-C. Similarly, pyrite was only quantified in the bottom layer TI-D where it represents 2.1% of the mineral content. In spite of this, very well preserved and euhedral crystals of sulfides could be also observed by SEM/EDS in the uppermost part of the profile. Secondary minerals consist of gypsum, anglesite, and a wide variety of hydrated Fe sulfates like rozenite, szomolnokite, mereiterite, melanterite and voltaite. Gypsum is one of the more abundant secondary minerals in the profile, and it is particularly concentrated in the TI-B_2 layer. Jarosite was quantified in all layers of tailing I with the exception of TI-B_2. The proportion of jarosite in the profile varies from 2.4% in TI-C to 4.5% in TI-A.

Primary minerals identified in sediments accumulated in tailing IV are quartz, Illite, K-feldspar and plagioclase, while sulfides were not identified by XRD. Secondary minerals are mostly gypsum and jarosite (see Supplementary Fig. 1 for X-ray diffractograms). Unlike tailing I, Fe (hydrous)sulfates were not detected in these layers.

The mineralogical composition of the efflorescences was also determined. Detritic minerals identified in the yellow crust were quartz and K-feldspar, while evaporitic minerals mostly consisted of Ca, Mg, Mn, and Fe (hydrous)sulfates such as gypsum, apjohnite, epsomite, and pickeringite (see Supplementary Fig. 3 for X-ray diffractograms). The mineralogy of the red coatings that cover the exposed walls of tailings is dominated by secondary sulfates such as gypsum, jarosite, and melanterite. About 5% of the total mineral content corresponds to the sulfoarsenate beudantite. Detritic minerals consisted of quartz and illite. Finally, blue aggregates were found in tailing IV. They are composed of sulfates such as gypsum, mereiterite, and romerite. Some oxides such as rutile and ilmenite, along with some crystals of unaltered arsenopyrite were also identified by SEM/EDS.

4.4. Phase associations

The proportions of As associated with the extracted solid phases (Table 1) are shown in Table 4. The amount of As associated with the soluble fraction in layers of tailing I varies between 1 to 24% of the near-total As with the highest values measured in the layer TI-B. In tailing IV, the proportion of the soluble fraction accounts for only 0.1% of the near-total As all along the profile.

Unlike the weakly adsorbed As, the proportion of the strongly adsorbed As is important in both profiles; in the profile of tailing I, it accounts for 17–41% of the near-total As concentration, while in tailing IV the proportion of strongly adsorbed As ranges between 10–37%. Arsenic associated with the more amorphous Fe (III) (hydr)oxide phases such as ferrihydrite and schwertmannite, represents about 3 to 8% of the near-total As concentration in tailing I, while in tailing IV this proportion varies between 0 and 17%. The fraction of As associated with crystalline Fe(III) oxides such as goethite and hematite but also with Fe oxyhydroxysulfates such as jarosite, is also important in both profiles, accounting for 2–31% in tailing I and 13–24% in tailing IV. The proportion of As associated with primary sulfides is variable in the profile T-I, while in T-IV the values are rather constant in depth. The residual fraction includes all phases that are not soluble in the reactives used in the described steps of extraction. The proportion of As associated with this fraction represents 17 to 30% of the near-total content of As measured in each layer of T- I and 13 to 45% in T-IV.

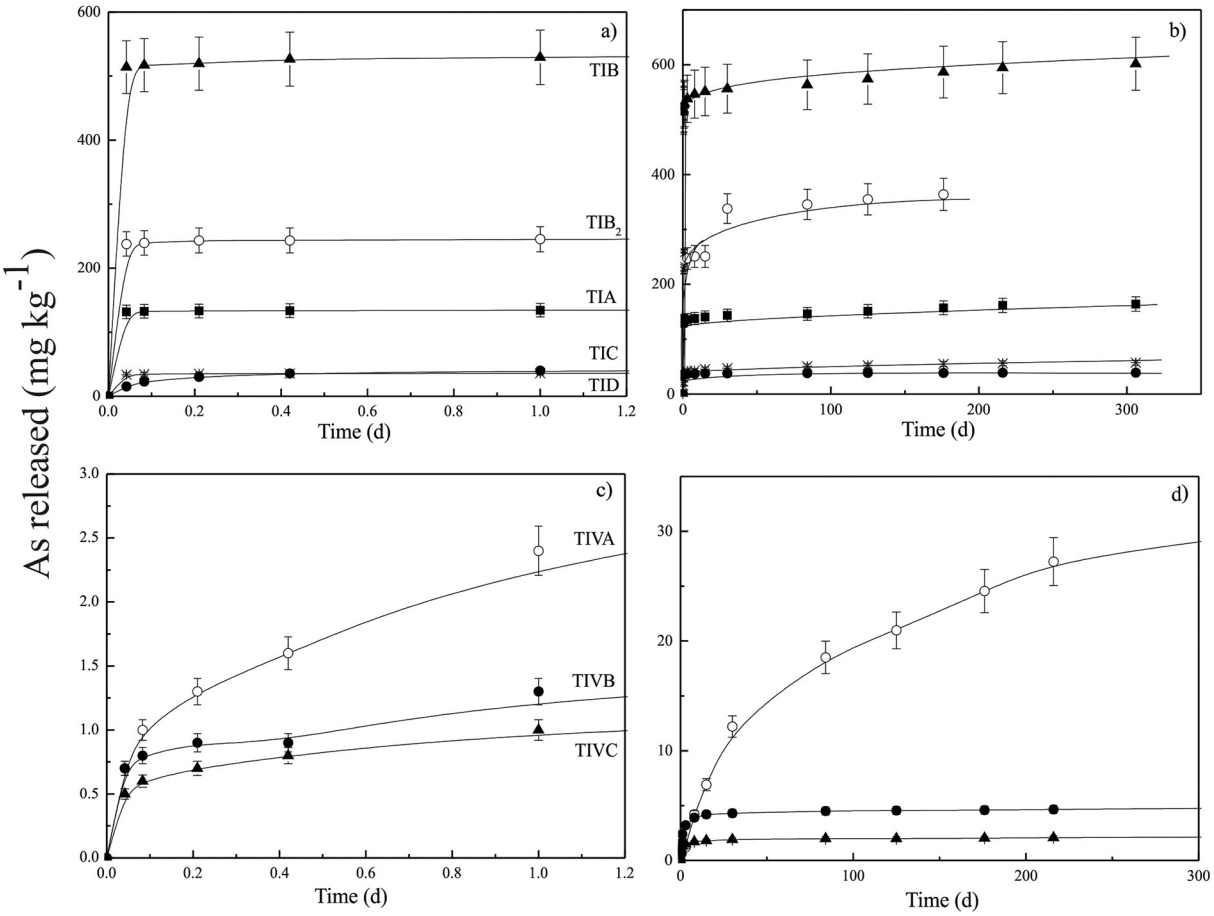

Fig. 3. Release of As with time measured in suspensions of sediments sampled from a) tailing I; and b) tailing IV in MilliQ water. The curves drawn through the measured points are indicative only of the general trend followed by the samples. Error bars correspond to ±standard deviation of duplicate sample measurements.

4.5. Release of As with time

Fig. 3 illustrates the results obtained in the experiments performed with the suspensions of the studied wastes. Fig. 3a and c show the results obtained from the beginning until the first 1.2 days of sediment–water interaction, while the complete trend is shown in Fig. 3b and d. As indicated in Fig. 3b, the highest release of As is derived from leachings of the layers TI-B and TI-B_2, followed by TI-A. On the contrary, the amounts of As released after 306 days of sediment–water interaction from the bottom layer and the intermediate layer TI-C were markedly lower and represented less than 4% of the near-total content of As. Another important feature observed in these experiments is that the release of As from suspensions of TI-A, TI-B and TI-B_2 during the first 60 min is remarkably high, while in the suspensions of TI-C and TI-D is much lower (Fig. 3a). The As released in the first hour of water-sediment interaction is equivalent to the As concentrations associated with the soluble fraction in the sequential extraction procedure. This initial release is followed by a slow liberation of As that suggests that the dissolution of a readily soluble As-bearing phase is reaching the equilibrium or that some other phases with slower dissolution rates are also contributing As in minor proportions.

Unlike the behavior observed in layers of tailing I, the release of As from layers of tailing IV is more gradual, with As concentrations that slightly increase with time until reaching a pseudo-equilibrium condition after approximately 30 days in layers TIV-B and TIV-C, while in the upper layer TIV-A this condition has not been yet observed until 306 days of reaction (Fig. 3d). In all cases, the amounts of As released from sediments accumulated in this tailing were lower than those measured in tailing I, and represent less than 8% of the corresponding near-total contents of As. Higher releases were measured in suspensions of the uppermost layer (TIV-A), while the lowest was observed in the bottom layer TIV-C (Fig. 3d). Besides, the concentration of As released within the first hour of reaction was almost negligible (<0.4%) in the three layers.

5. Discussion

The release of As in MilliQ water from the sediments accumulated in tailing I occurs mostly within the first hour of sediment–water contact, and corresponds to the amount of As associated with water-soluble phases. There is a clear distribution of these water-soluble phases in the profile, as their higher proportions are concentrated in sediments accumulated above the hardpan level. When the concentrations of As released in the first hour of sediment–water interaction are compared with the near-total As concentration in each layer, it is clear that the release is not only conditioned by the content of near-total arsenic, but also seems to be mostly associated to the solubility and dissolution rate of the As-bearing phases present in the sediments (Fig. 4).

According to solubility values reported in the literature (e.g., Hammarstrom et al., 2005; Drahota and Filippi, 2009), the more soluble minerals contained in the weathering profiles and in the efflorescences of the study area correspond to a relatively wide variety of simple hydrated sulfates which have the general formula $M^{2+}SO_4 \cdot nH_2O$, where M = Fe^{2+}, Mg, and Ca, as well as mixed divalent–trivalent salts. The mechanism that explains the association of arsenic with these natural phases still remains uncertain. Nevertheless, detectable concentrations of

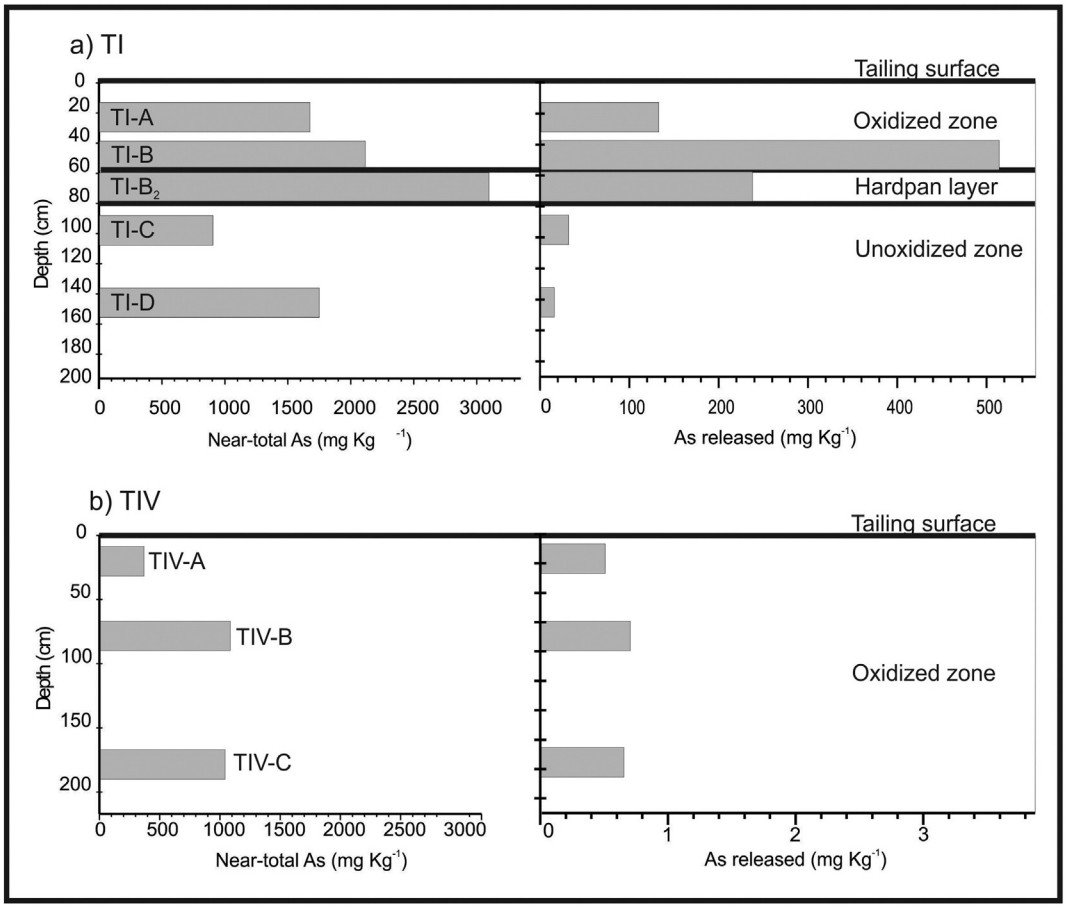

Fig. 4. Comparison between the near-total concentration of As and the amount of As released in suspensions of sediments in MilliQ water after 1 h of reaction. a) Tailing I; b) tailing IV. Note that the concentration of As released to water is not directly correlated with the total As content.

As have been reported in leachates of a number of natural hydrated sulfates such as rozenite ($FeSO_4 \cdot 4H_2O$), melanterite ($FeSO_4 \cdot 7H_2O$) and copiapite ($Fe^{2+}Fe^{3+}{}_4(SO_4)_6(OH)_2 \cdot 20H_2O$) (e.g., Valente and Gomes, 2009; Jamieson et al., 2005; Hammarstrom et al., 2005). In agreement, we have measured elevated concentrations of arsenic in the 1 h leachates of the efflorescences collected from the study area (Table 2) which are mostly composed of simple hydrated sulfates and sulfoarsenates (Table 3). Unlike tailing I, the release of As from the weathering profile

Table 3
Mineralogical composition of mine wastes and saline crusts.

Phases (%)	TI-A	TI-B	TI-B_2	TI-C	TI-D	TIV-A	TIV-B	TIV-C	Yellow	Red	Blue
	Tailing I					Tailing IV			Saline crusts		
Quartz (SiO_2)	65.6	47.6	57.2	71.1	57.0	71.6	49.0	51.9	12.7	64.0	45.8
Illite $K_{0.65}Al_2[Al_{0.65}Si_{3.35}O_{10}](OH)_2$	27.5	36.0	31.2	25.1	36.6	23.6	26.6	24.1		27.3	23.4
Gypsum ($CaSO_4 \cdot 2H_2O$)	1.0		6.2	<1.0	<1.0	2.8			6.8	<1.0	5.3
Albite ($NaAlSi_3O_8$)			1.7	<1.0			10.9	14.3			
Orthoclase ($KAlSi_3O_8$)							7.2	4.3			
Sanidine $(K,Na)(Si,Al)_4O_8$									21.6		
Jarosite $KFe_3(SO_4)_2(OH)_6$	3.4	3.7		2.4	2.5	2.0	6.3	3.8			
Plumbojarosite $PbFe_3(SO_4)_4(OH)_{12}$	1.2										
Voltaite $K_2(Fe^{2+})_5(Fe^{3+})_3Al(SO_4)_{12} \cdot 18H_2O$	<1.0	<1.0	<1.0								
Szomolnokite $FeSO_4 \cdot (H_2O)$		2.6									
Rozenite $FeSO_4 \cdot 4H_2O$		1.5	1.3								
Mereiterite $K_2Fe(SO_4)_2 \cdot 4(H_2O)$	1.1	7.0									4.7
Anglesite $PbSO_4$		<1.0	1.7								
Pyrite FeS_2					2.1						
Melanterite $FeSO_4 \cdot 7H_2O$					1.6					2.4	
Rhomboclase $H_5FeO_2(SO_4)_2 \cdot 2H_2O$								1.6			
Pickeringite $MgAl_2(SO_4)_4 \cdot 22(H_2O)$									<1.0		
Epsomite $MgSO_4 \cdot 7(H_2O)$									11.0		
Apjohnite $MnAl_2(SO_4)_4 \cdot 22H_2O$									47.5		
Beudantite $PbFe(AsO_4)(SO_4)(OH)_6$										5.4	
Romerite $Fe^{2+}Fe_2^{3+}(SO_4)_4 \cdot 14H_2O$											6.5
χ^2	1.80	1.72	1.86	1.99	1.57	1.65	2.17	2.09	2.37	1.63	1.92

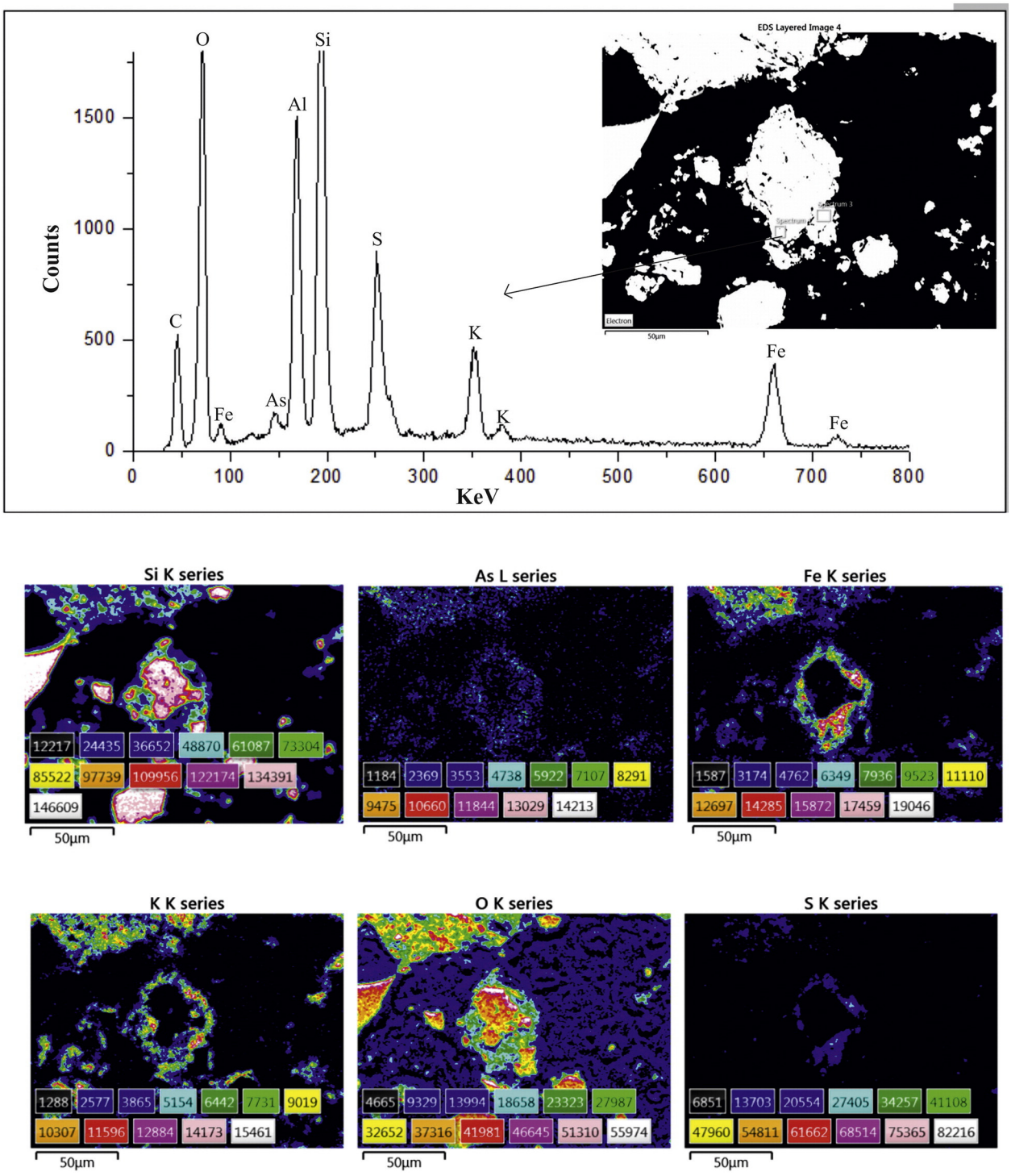

Fig. 5. SEM image and EDS spectra showing the chemical composition of As-jarosite rim in the TI-B sample. X-ray mappings show the spatial distribution of Si, As, Fe, K, O and S. Color scale represents elemental intensity. (For interpretation of the references to color in this figure legend, the reader is referred to the web version of this article.)

formed in tailing IV is almost negligible, in consonance with the occurrence of relative low proportions of the more soluble (hydrous)sulfate minerals (Table 3).

As-jarosite is relatively abundant in our system (Table 3, Fig. 5) and although its rate of dissolution in acid and oxic conditions is low, leaching tests performed at pH 2 with synthesized As-jarosites indicate a rapid increase in As aqueous concentrations during the first few days of dissolution (Kendall et al., 2013). Therefore, some contribution from As-jarosite to the pool of As associated to the water soluble fraction is also expected. The mechanism of incorporation of As in jarosite is well understood and occurs via the substitution of sulfate for arsenate (i.e., Paktunc and Dutrizac, 2003; Savage et al., 2005; Morin and Calas, 2006; Smith et al., 2006; Basciano and Peterson, 2007; Johnston et al., 2012).

In spite of the elevated proportion of strongly adsorbed As measured in the tailings profiles (Table 4), the contribution to the pool of soluble As from desorption is considered to be minor because at the equilibrium pHs of the suspensions ($pH_{eq} < 5$) the As(V) adsorption onto Fe(hydr) oxides is maximum (i.e., Pierce and Moore, 1982; Goldberg, 1986;

Table 4
Results of sequential extraction of mine tailings TI and TIV. Values correspond to As proportions expressed in wt.%.

Sample	Soluble	Weakly adsorbed As	Strongly adsorbed As	Fe(III) oxy-hydroxides	Fe(III) oxides	Primary sulfides	Residual
TI							
TI-A	8	0	41	5	18	11	17
TI-B	24	0	38	3	2	1	31
TI-B_2	8	0	32	3	3	24	30
TI-C	4	0	36	7	31	0	22
TI-D	1	1	17	8	20	22	30
TIV							
TIV-A	0.1	0	11	0	24	19	45
TIV-B	0.1	0	10	4	21	22	42
TIV-C	0.1	0	37	17	13	20	13

Fuller et al., 1993; Mamindy-Pajany et al., 2009). Therefore, As adsorbed onto the Fe oxides phases is considered to be almost immobile under the pH and redox conditions predominating in the system.

6. Conclusions

The sulfide-rich residues of La Concordia mine are accumulated in four tailing dams that remained exposed to the weathering agents for almost 30 years. In such period of time, a complex sequence of redox and dissolution/precipitation reactions occurred, leading to the gradual oxidation of the original waste and the formation of weathering profiles. Sulfide oxidation also originated a typical acid mine drainage, rich in dissolved metal(oid)s and sulfate, that leaks into La Concordia, the small creek that crosses the site. As a consequence, the water quality is strongly affected, as it shows acidic pH values (i.e., pH < 4) and concentrations of metals and arsenic that highly exceed the guidelines values for drinking water.

Climatic conditions dominating in the entire Puna plateau as well as the secondary minerals that precipitate in sites affected by AMD, play an important role in the mobility of this pollutant. Due to the intense evaporation, a wide variety of As-bearing sulfates precipitate from As, Fe and SO_4^{2-} rich solutions that result from sulfide oxidation. These salts show a wide range of solubility and therefore its role in controlling the partition of As between the solid and aqueous phases is variable. The more soluble phases that may retain As are (hydrous)sulfate that precipitate forming large saline crusts or aggregates disseminated within the sediments matrix. The role of these minerals as sinks of As is only temporally effective because they rapidly dissolve during the occasional rainfall events releasing As to the water. Less soluble As-bearing phases identified in the wastes, such as As-jarosite and beudantite may also contribute As to the water in longer periods of sediment–water interaction. In addition, an important proportion of As remains adsorbed onto Fe (hydr)oxides thus representing a hazardous reservoir with the potential of mobilizing As into porewaters and streamwaters if the acidic and oxidizing conditions dominating the region are altered. Regarding the concentrations of As measured in La Concordia Creek, it seems that the retention of As into these solid phases is not effective enough to meet the As requirements for drinking water.

Acknowledgments

Authors wish to acknowledge the assistance of CONICET and UNC whose support facilities and funds (PIP 112-201101-00251 and 112-201101-00326 and SECYT 203/2014) were used in this investigation. N.E. Nieva acknowledges a doctoral fellowship from CONICET. L. Borgnino, F. Locati and M.G. Garcia are members of CICyT in CONICET, the National Science Foundation of Argentina. Thanks to Andrea Lojo for the ICP-MS analysis and to Maximiliano Medina for the preparation of polished thin sections for SEM/EDS analysis. We are especially grateful to the Associate Editor and one anonymous reviewer for carefully reading this work and suggesting significant improvements to a former version of this manuscript.

Appendix A. Supplementary data

Supplementary data associated with this article can be found in the online version, at http://dx.doi.org/10.1016/j.scitotenv.2016.01.147. These data include the Google map of the most important areas described in this article.

References

Argañaraz, R., Mancini, J., Sureda, R., 1982. El yacimiento de Concordia (Ag-Pb) en la provincial de Salta, Argentina. Un proyecto de rehabilitacion y explotacion minera. 5° Congreso Latinoamericano de Geologia, Actas 5, 61–78.
Basciano, L.C., Peterson, R.C., 2007. Jarosite–hydronium jarosite solid-solution series with full iron site occupancy: mineralogy and crystal chemistry. Am. Mineral. 92, 1464–1473.
Bigham, J.M., Nordstrom, D.K., 2000. Iron and aluminum hydroxysulfates from acid sulfate waters. In: Alpers, C.N., Jambor, J.L., Nordstrom, D.K. (Eds.), Sulfate Minerals—Crystallography, Geochemistry, and Environmental Significance. Rev. Mineral. Geochem. 40, pp. 351–403.
CAA Código Alimentario Argentino, 2007. Capitulo XII. Bebidas Hídricas, Agua y Agua Gasificada. Artículo 982. Res Conj. SPRyRS y SAGPyA N° 68/2007 y N° 196/2007. Ley 18284. Buenos Aires, Marzocchi.
Carlson, L., Bigham, J.M., Schwertmann, U., Kyek, A., Wagner, F., 2002. Scavenging of As from acid mine drainage by schwertmannite and ferrihydrite: a comparison with synthetic analogues. Environ. Sci. Technol. 36, 1712–1719.
Coira, B., Viramonte, J., 1999. Volcanismo básico plioceno-reciente de trasarco en la Puna austral. In: Bonorino, G. González, Omarini, R., Viramonte, J. (Eds.), Geología del Noroeste Argentino. XIV Congr. Geol. Arg. Relatorio 1, pp. 397–399.
Coira, B., Kay, S., Viramonte, J., 1993. Upper Cenozoic magmatic evolution of the Argentine Puna — a model for changing subduction geometry. Int. Geol. Rev. 35, 677–720.
Dold, B., 2003. Speciation of the most soluble phases in a sequential extraction procedure adapted for geochemical studies of copper sulfide mine waste. J. Geochem. Explor. 80, 55–68.
Drahota, P., Filippi, M., 2009. Secondary arsenic minerals in the environment: a review. Environ. Int. 35, 1243–1255.
Frau, F., 2000. The formation-dissolution-precipitation cycle of melanterite at the abandoned pyrite mine of Genna Luas in Sardinia, Italy: environmental implications. Mineral. Mag. 64, 995–1006.
Fuller, C.C., Davis, J.A., Waychunas, G.A., 1993. Surface chemistry of ferrihydrite: part 2. Kinetics of arsenate adsorption and coprecipitation. Geochim. Cosmochim. Acta 57, 2271–2282.
Goldberg, S., 1986. Chemical modeling of arsenate adsorption on aluminum and iron oxide minerals. Soil Sci. Sot. Amer. J. 50, 1154–1160.
Hammarstrom, J.M., Seal, R.R., Meier, A.L., Kornfeld, J.M., 2005. Secondary sulfate minerals associated with acid drainage in the eastern US: recycling of metals and acidity in surficial environments. Chem. Geol. 215, 407–431.
Jamieson, H.E., 2011. Geochemistry and mineralogy of solid mine waste: essential knowledge for predicting environmental impact. Elements 7, 381–386.
Jamieson, H., Robinson, C., Alpers, C.N., McCleskey, R.B., Nordstrom, D.K., Peterson, R.C., 2005. Major and trace element composition of copiapite-group minerals and coexisting water from the Richmond mine, Iron Mountain, California. Chem. Geol. 215, 387–405.
Johnston, S.G., Burton, E.D., Keene, A.F., Planer-Friedrich, B., Voegelin, A., Blackford, M.G., Lumpkin, G.R., 2012. Arsenic mobilization and iron transformations during sulfidization of As(V)-bearing jarosite. Chem. Geol. 334, 9–24.
Kendall, M.R., Madden, A.S., Elwood Madden, M.E., Hu, Q., 2013. Effects of arsenic incorporation on jarosite dissolution rates and reaction products. Geochim. Cosmochim. Acta 112, 192–207.
Keon, N.E., Swartz, C.H., Brabander, D.J., Harvey, C., Hemond, H.F., 2001. Validation of an arsenic sequential extraction method for evaluating mobility in sediments. Environ. Sci. Technol. 35, 2778–2784.

Kirschbaum, A., Murray, J., Arnosio, M., Tonda, R., Cacciabue, L., 2012. Pasivos ambientales mineros en el noroeste de Argentina: aspectos mineralógicos, geoquímicos y consecuencias ambientales. Revista Mexicana de Ciencias Geológicas 29, 248–264.

Langmuir, D., Mahoney, J., MacDonald, A., Rowson, J., 2006. Solubility products of amorphous ferric arsenate and crystalline scorodite (FeAsO42H2O) and their application to arsenic behavior in buried mine tailings. Geochim. Cosmochim. Acta 70 (12), 2942–2956.

Lottermoser, B.G., 2010. Mine Wastes: Characterization, Treatment and Environmental Impacts. third ed. Springer, Berlin, Heidelberg, p. 400.

Lottermoser, B.G., Ashley, P.M., 2006. Physical dispersion of radioactive mine waste at the rehabilitated Radium Hill uranium mine site, South Australia. Aust. J. Earth Sci. 53, 485–499.

Mamindy-Pajany, Y., Hurel, C., Marmier, N., Roméo, M., 2009. Arsenic adsorption onto hematite and goethite. Comptes rendus – Chimie 8, 876–881.

Matteini, M., Mazzuoli, R., Omarini, R., Cas, R., Maas, R., 2002. The geochemical variations of the upper Cenozoic volcanism along the Calama–Olacapato–El Toro trasnversal fault system in central Andes (24°S): petrogenetic and geodynamic implications. Tectonophysics 345, 211–227.

Morin, G., Calas, G., 2006. Arsenic in soils, mine tailings, and former industrial sites. Elements 2, 97–101.

Nordstrom, D.K., Alpers, C.N., 1999. Geochemistry of acid mine waste. In: Plumlee, G.S., Londgson, M.J. (Eds.), The Environmental Geochemistry of Ore Deposits. Part A: Processes, Techniques, and Health Issues. Reviews in Economic Geology, pp. 133–160.

Paktunc, D., Dutrizac, J.E., 2003. Characterization of arsenate-for-sulfate substitution in synthetic jarosite using X-ray diffraction and X-ray diffraction and X-ray absorption spectroscopy. Can. Mineral. 41, 905–919.

Pesce, A.H., Miranda, F., 2003. Catálogo de manifestaciones termales de la Republica Argentina. Volumen 1-Region Noroeste 36. SEGEMAR, Buenos Aires, pp. 1666–3462.

Petrinovic, I.A., Mitjavila, J., Viramonte, J.G., Marti, J., Becchio, R., Arnosio, M., Colombo, F., 1999. Geoquímica y Geocronología de secuencias volcánicas Neógenas de trasarco, en el extremo oriental de la Cadena Volcánica Transversal del COT, noroeste de Argentina. In: Colombo, F., Queralt, I., IA, Petrinovic (Eds.), Geología de los Andes Centrales Meridionales: El Noroeste Argentino. Acta Geológica Hispánica 34, pp. 255–273.

Pierce, M.L., Moore, C.B., 1982. Adsorption of arsenite and arsenate on amorphous iron hydroxide. Water Res. 16, 1247–1253.

Riller, U., Petrinovic, I.A., Ramelow, J., Greskowiak, J., Strecker, M., Oncken, O., 2001. Late Cenozoic tectonism, caldera and plateau formation in the central Andes. Earth Planet. Sci. Lett. 188, 299–311.

Savage, K., Bird, D., O'Day, P., 2005. Arsenic speciation in synthetic jarosite. Chem. Geol. 215, 473–498.

Smedley, P.L., Kinniburgh, D.G., 2002. A review of the source, behaviour and distribution of arsenic in natural water. Appl. Geochem. 17, 517–568.

Smith, A., Dubbin, W., Wright, K., Hudson-Edwards, K., 2006. Dissolution of lead- and lead arsenic-jarosite at pH 2 and 8 and 20 °C: insights from batch experiments. Chem. Geol. 229, 344–361.

Valente, T.M., Gomes, C.L., 2009. Occurrence, properties and pollution potential of environmental minerals in acid mine drainage. Sci. Total Environ. 407, 1135–1152.

WHO World Health Organization, 2004. Guidelines for drinking — water quality. third ed. Recommendations vol. 1 (Geneva).

Zappettini, E.O., 1990. Mineralizaciones polimetálicas de los distritos El Queva, La Poma-Incacchule y Concordia, Salta. In: Zappettini, E.O. (Ed.), Recursos minerales de la República ArgentinaAnales 35. Instituto de Geología y Recursos Minerales (SEGEMAR), pp. 1603–1611.